CHAPTER 7

MEASUREMENT OF ACTIVATION ENERGIES FOR ETHYLENE DIELS-ALDER-DEHYDRATION REACTIONS

This chapter provides a summary and discussion of kinetic data obtained for two different Diels-Alder-dehydration reactions catalyzed by the Lewis acid molecular sieve, Zr-Beta: (1) the synthesis of PX from DMF and ethylene, and (2) the synthesis of MPT from MMF and ethylene (Fig. 7.1).

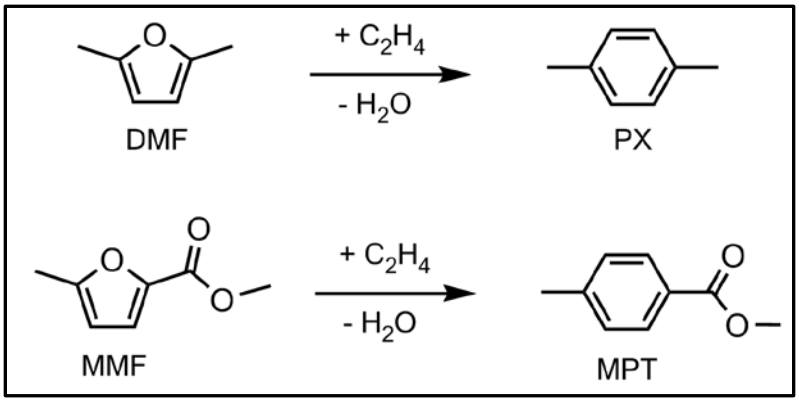

Fig. 7.1 Ethylene Diels-Alder-dehydration reactions of DMF to PX and MMF to MPT.

Each system was investigated by first determining whether the kinetics of the Diels-Alder-dehydration reactions were influenced by mass transfer limitations within the molecular sieve catalysts. This was determined by performing the Madon-Boudart test and plotting the initial rates of product formation versus varying active site content in the catalyst. The Madon-Boudart criterion states that if the initial rates are linear with the number of active sites in different crystalline microporous catalyst samples of constant crystal size, then

the transport of the reactant molecule to the catalytic active site is not limiting the rate of reaction.[1] Here, the test is performed based on the assumption that all Zr metal atoms in the Zr-Beta catalysts are equally active and accessible active sites for the Diels-Alder-dehydration reaction. It is critical to determine if transport limitations are present before measuring any further kinetics of a reaction. If transport of the reactant to the active site is limiting, any measured activation energy will not be characteristic of the chemical reaction over the catalyst being studied. Therefore, this makes it impossible to compare the effect different catalysts have on the actual rate of chemical reaction.

After determining if measured reaction rates were influenced by transport limitations for both reactions, the initial rates of product formation using Zr-Beta were measured at different reaction temperatures to generate Arrhenius plots. Apparent activation energies of reaction using the Zr-Beta catalyst were then determined from the slopes of these plots. The results for the synthesis of PX from DMF and ethylene will be discussed first, followed by a discussion of the results for the production of MPT from MMF and ethylene.

7.1 Synthesis of PX from DMF and ethylene with Zr-Beta catalyst

A series of four Zr-Beta samples of varying Si/Zr atomic ratios were prepared by methods described in Chapter 2. The Zr source used in the syntheses was Zr(IV) propoxide. Table 7.1 summarizes the Si/Zr ratios and crystal size of each sample used in the investigation.

Table 7.1 Zr-Beta sample characterization. Each sample was highly crystalline as determined by XRD, and scanning electron microscopy (SEM) images indicated nearly constant crystal size among all samples (see appendix Fig. 7.1-8-A). Elemental composition was determined by Galbraith Laboratories (GLI procedure ME-70).

Sample name	Si/Zr atom ratio	Crystal size (µm)
Zr-Beta-92	92	0.75 - 1.0
Zr-Beta-155	155	0.75 - 1.0
Zr-Beta-264	264	1.0 - 1.25
Zr-Beta-492	492	0.75 - 1.0

To determine whether transport limitations within the microporous Zr-Beta catalysts were influencing the measured rates of PX production from DMF and ethylene in dioxane solvent, the initial rates of PX production were measured as function of Zr content in the catalyst. The PX yield profiles using the four Zr-Beta catalysts were collected at 230^{o}C (Fig. 7.2) and initial rates (t = 0) were determined (Table 7.2).

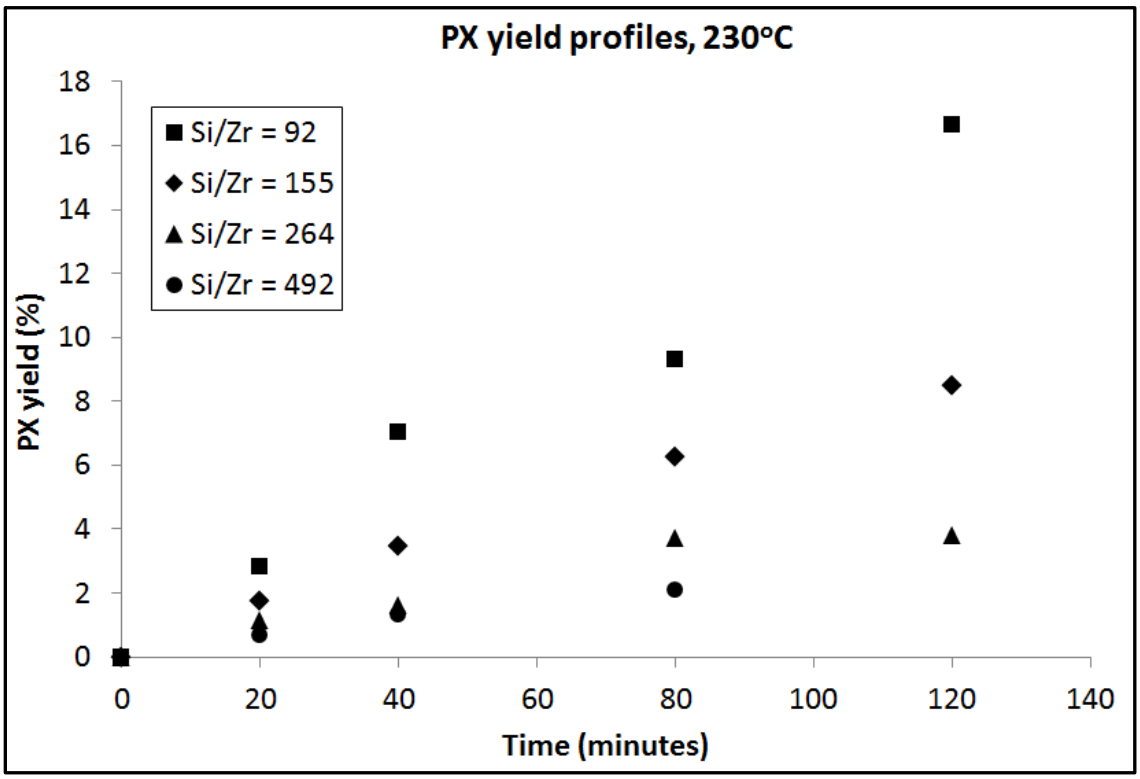

Fig. 7.2 PX yield profiles for Diels-Alder-dehydration of DMF and ethylene using Zr-Beta catalysts with varying Si/Zr molar ratios. Reaction conditions: 0.1 M DMF in dioxane, 0.1 M triglyme (internal standard), 30 mg catalyst, 230°C, 35 bar C_2H_4 (room temperature).

Table 7.2 Initial rates of PX formation for profiles in Fig. 7.2.

		Initial rate (mM PX/hr)		
Si/Zr	**Zr (mmol)**	Min	Max	Average
92	0.0054	8.40	10.68	9.54
155	0.0032	5.16	5.22	5.19
264	0.0019	2.40	3.30	2.85
492	0.0010	1.86	1.98	1.92

The initial rates were determined by simply estimating the slope of the profiles at initial time (t=0 min). The data displayed a small amount of scatter that can be attributed to the separate batch reaction experiments required to collect

each individual data point. To account for the scatter in estimating the initial rates, a “maximum” and “minimum” slope was drawn for each profile and the “average” initial rate was the average of these two slopes. See the methods section in this chapter for experimental details.

The measured initial PX production rates (in mM PX/hr) are plotted against the Zr content in the catalyst (using 30 mg of catalyst loading) in Fig. 7.3. The initial rate of PX production is clearly linear with the amount of Zr in the catalyst for the four Zr-Beta materials tested. If the assumption holds true that each Zr atom is equal, active, and accessible, then the possibility of a transport limitation influencing the measured kinetics at temperatures up to 230^{o}C may now be neglected.

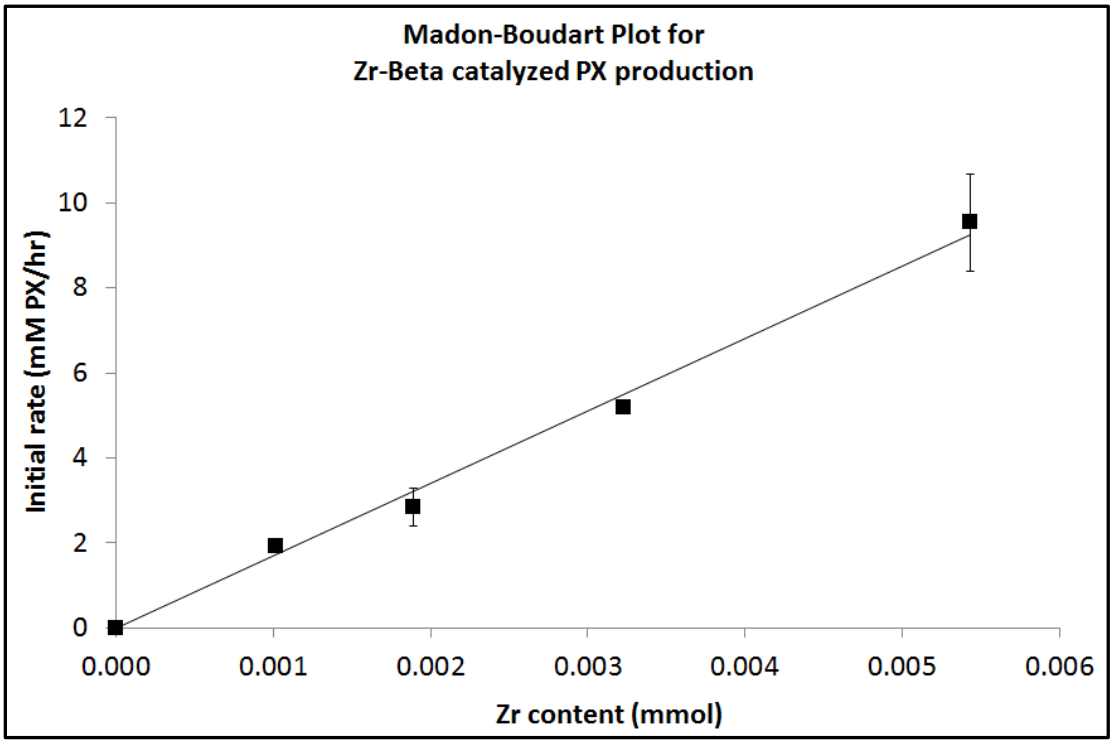

Fig. 7.3 Madon-Boudart plot for Zr-Beta catalyzed PX production at 230^{o}C. The error bars are the max/min slopes of the PX yield profiles (see Chap. 7 methods section).

Next, an apparent activation energy (E_a) for the conversion of DMF and ethylene to PX using Zr-Beta was measured. The PX yield profiles were collected at four different temperatures (170, 190, 210, and 230 ^{o}C) using the sample Zr-Beta-155 (Fig. 7.4.). The same procedure was applied to measure the initial rates (Table 7.3).

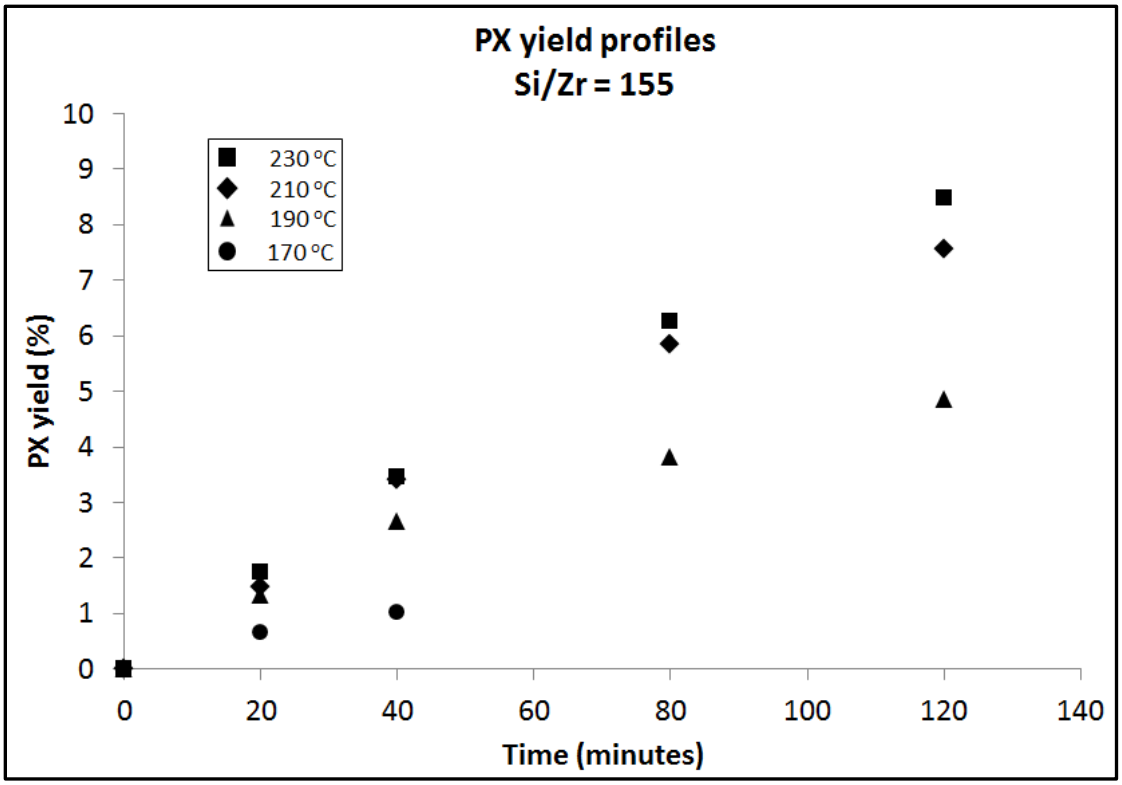

Fig. 7.4 PX yield profiles for Diels-Alder-dehydration of DMF and ethylene using Zr-Beta-155 with varying reaction temperature. Reaction conditions: 0.1 M MMF in dioxane, 0.1 M triglyme (internal standard), 30 mg Zr-Beta-155, 35 bar C_2H_4 (room temperature).

Table 7.3 Initial rates of PX formation for profiles in Fig. 7.4.

	Initial rate (mM PX/hr)		
T (^{o}C)	Min	Max	Average
230	5.16	5.22	5.19
210	4.44	5.16	4.80
190	3.78	4.02	3.90
170	1.56	2.04	1.80

An Arrhenius plot was generated from the data (Fig. 7.5) and the apparent E_a determined by the slope of a fitted line through the four points is 8.2 kcal/mol. Since it appears that the slope of the plot may be different at the low and high temperature ranges, apparent E_a's corresponding to the different slopes were also measured (Fig. 7.6 and Fig. 7.7). In the 170-210 ^{o}C range the apparent E_a is 10.5 kcal/mol and in the 210-230 ^{o}C range an apparent E_a of only 1.9 kcal/mol is measured.

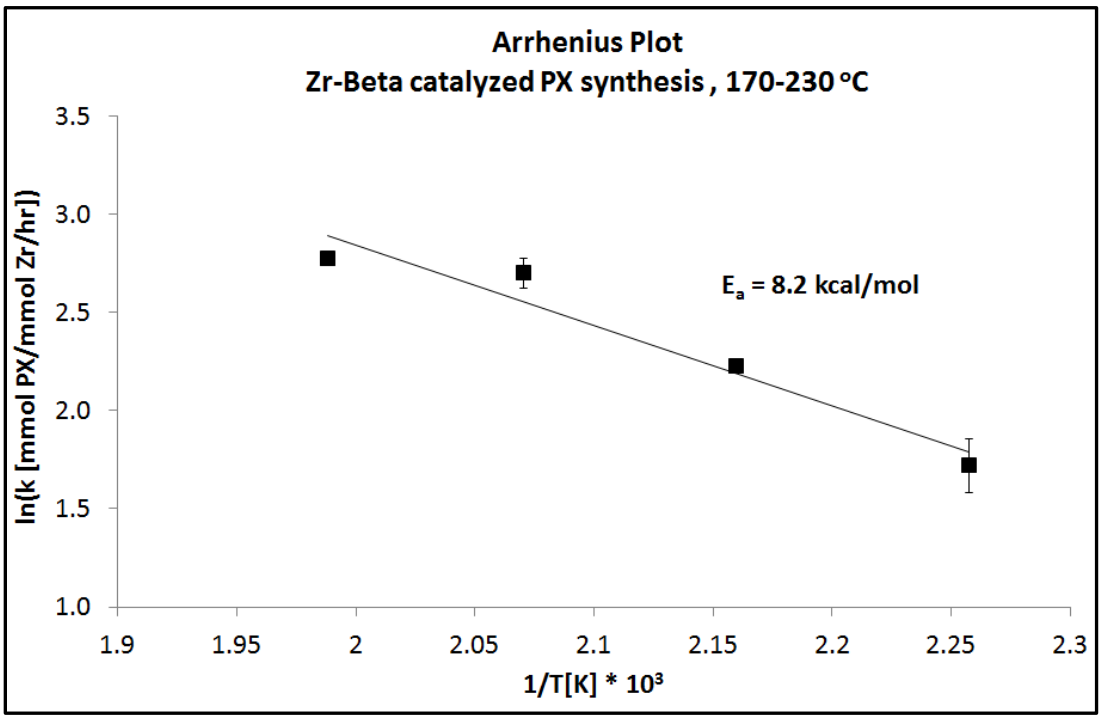

Fig. 7.5 Arrhenius Plot for Zr-Beta catalyzed PX synthesis for 170-230^{o}C.

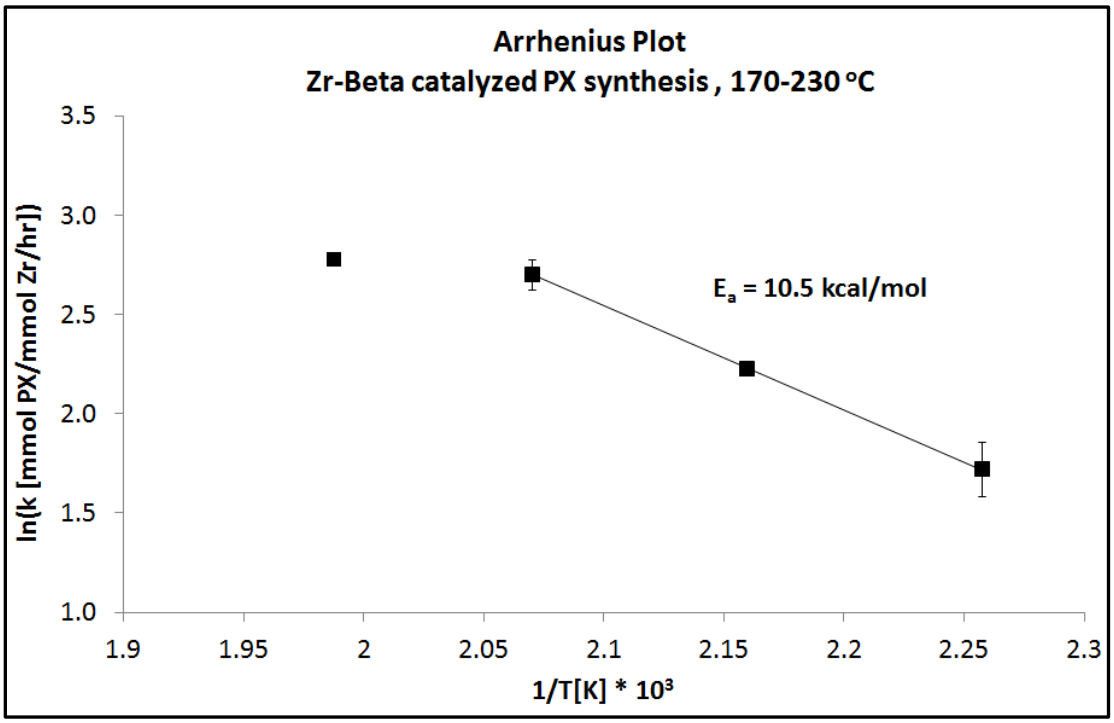

Fig. 7.6 Arrhenius Plot for Zr-Beta catalyzed PX synthesis for 170-230 ^{o}C. Apparent E_a = 10.5 kcal/mol reported for low temperature range (170-210 ^{o}C).

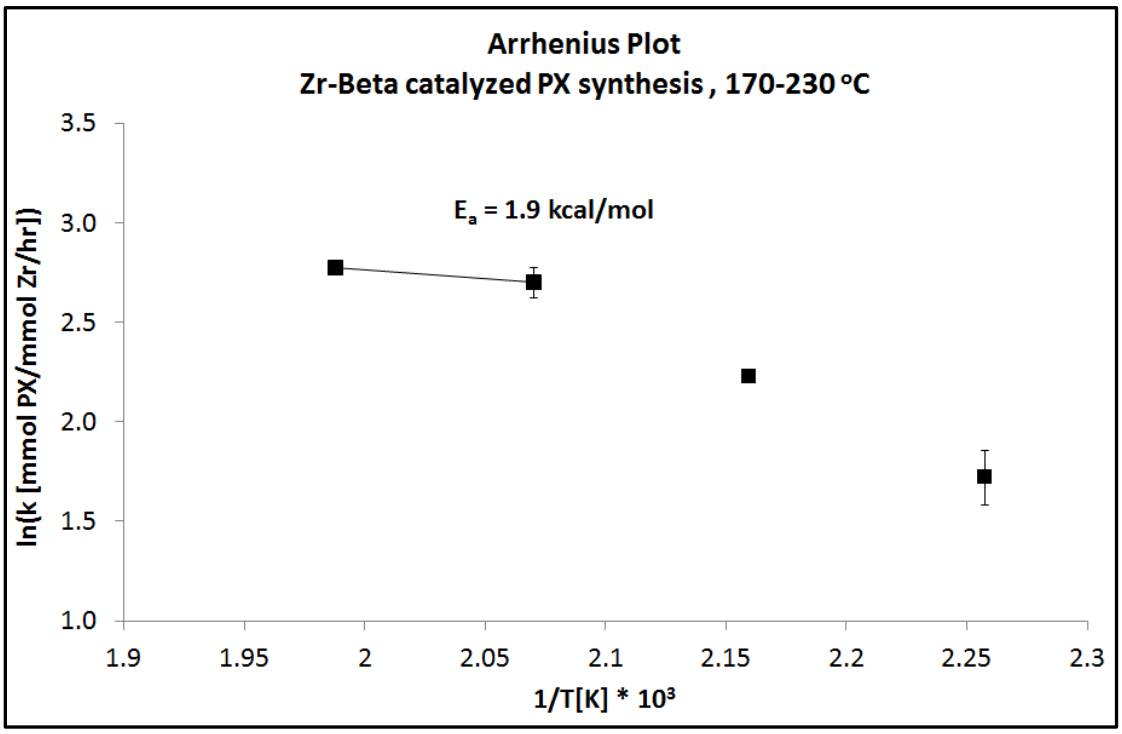

Fig. 7.7 Arrhenius Plot for Zr-Beta catalyzed PX synthesis for 170-230 ^{o}C. Apparent E_a = 1.9 kcal/mol reported for high temperature range (210-230 ^{o}C).

7.2 Synthesis of MPT from MMF and ethylene with Zr-Beta catalyst

To compare with the DMF/PX system, a nearly identical analysis was performed for the Zr-Beta catalyzed Diels-Alder-dehydration reaction of MMF and ethylene to MPT. Refer to the methods section in this chapter for experimental details.

MPT yield profiles were collected using the four Zr-Beta samples at 230^{o}C (Fig. 7.8) and initial rates were estimated (Table 7.4). The initial rates using each sample are plotted against the Zr content in the catalyst to generate a Madon-Boudart plot (Fig. 7.9). The Madon-Boudart plot appears to be non-linear, especially with the highest Zr content catalyst (Zr-Beta-92), indicating a possible diffusion limitation. Since the lowest Zr content catalyst (Zr-Beta-492) has a large uncertainty (larger error bars) and the middle two catalysts (Zr-Beta-264, Zr-Beta-155) look to be linear with (0,0), the first three catalysts (Zr-Beta-492, Zr-Beta-264, and Zr-Beta-155) may not be diffusion limited. The line on the plot is the trendline for the first three points passing through (0,0). Additional experiments are required to know the true shape of the plot and to have more confidence in knowing whether a diffusion limitation exists.

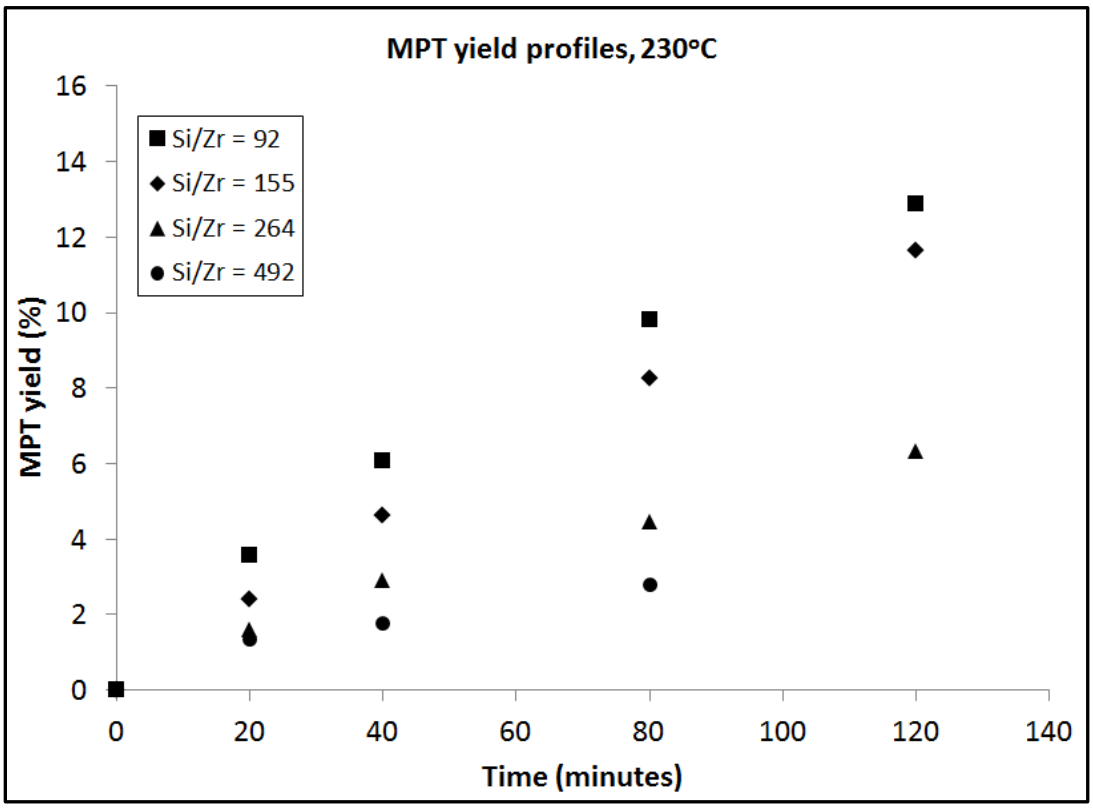

Fig. 7.8 MPT yield profiles for Diels-Alder-dehydration of MMF and ethylene using Zr-Beta catalysts with varying Si/Zr molar ratios. Reaction conditions: 0.1 M MMF in dioxane, 0.1 M triglyme (internal standard), 100 mg catalyst, 230^{o}C, 35 bar C_2H_4 (room temperature).

Table 7.4 Initial rates of MPT formation for profiles in Fig. 7.8.

		Initial rate (mM MPT/hr)		
Si/Zr	**Zr (mmol)**	Min	Max	Average
92	0.018	9.00	10.62	10.35
155	0.011	6.84	7.20	7.02
264	0.006	4.32	4.86	4.59
492	0.003	2.70	3.96	3.33

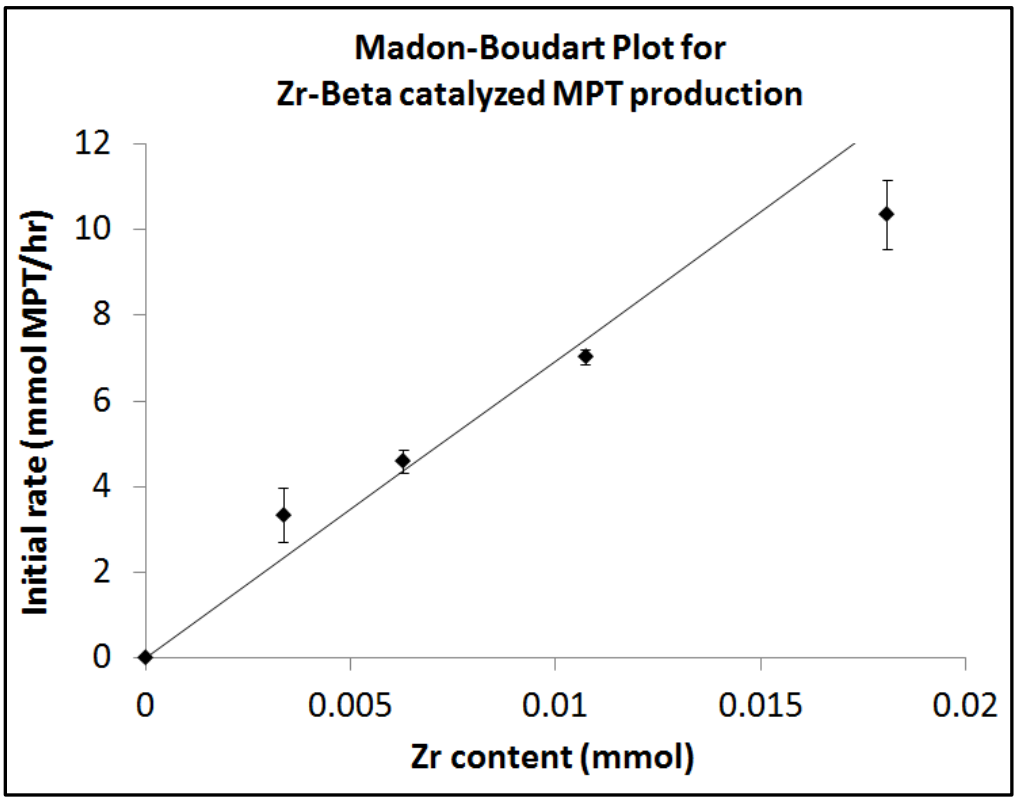

Fig. 7.9 Madon-Boudart plot for Zr-Beta catalyzed MPT production at 230^{o}C. The error bars are the max/min slopes of the MPT yield profiles (see Chap. 7 methods section).

The MPT yield profiles were collected at five different temperatures (170, 190, 210, 220, and 230 ^{o}C) using the sample Zr-Beta-155 (Fig. 7.10) and the initial rates were estimated (Table 7.5). An Arrhenius plot was generated from the data (Fig. 7.11) and the apparent E_a determined by the slope of a fitted line through the five points is 6.4 kcal/mol.

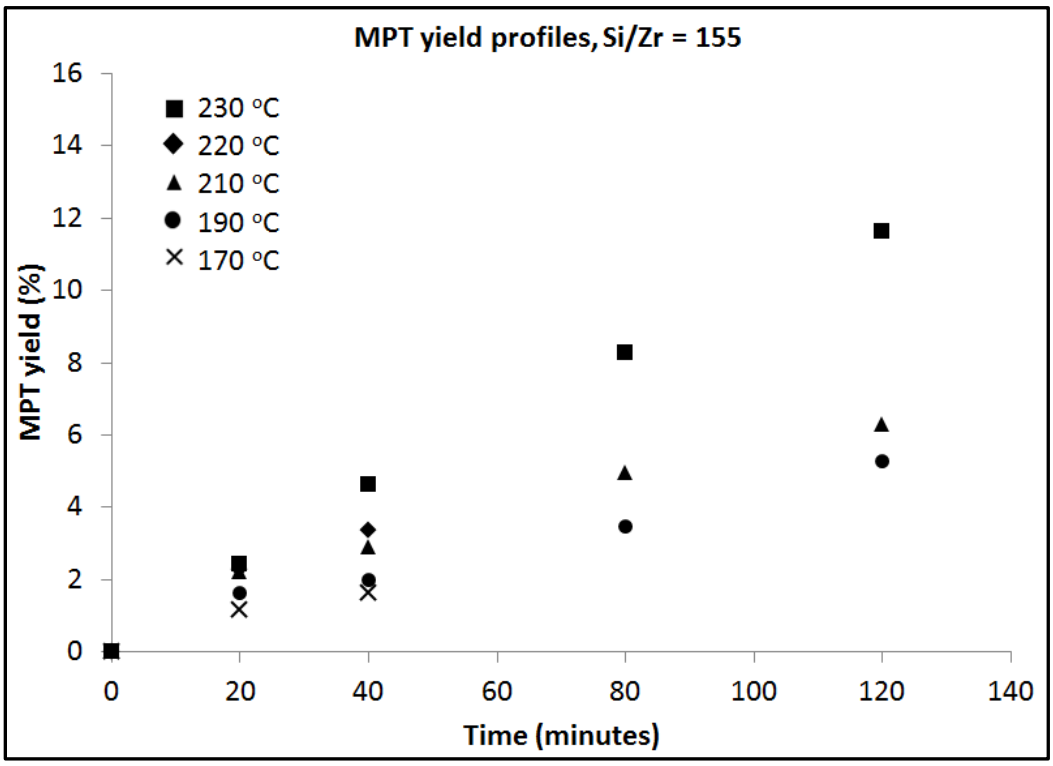

Fig. 7.10 MPT yield profiles for Diels-Alder-dehydration of MMF and ethylene using Zr-Beta-155 with varying reaction temperature. Reaction conditions: 0.1 M MMF in dioxane, 0.1 M triglyme (internal standard), 100 mg Zr-Beta-155, 35 bar C_2H_4 (room temperature).

Table 7.5 Initial rates of MPT formation for profiles in Fig. 7.10.

	Initial rate (mM MPT/hr)		
T (°C)	Min	Max	Average
230	6.84	7.38	7.11
220	5.04	6.84	5.94
210	4.32	6.48	5.40
190	2.88	5.04	3.96
170	2.52	3.42	2.97

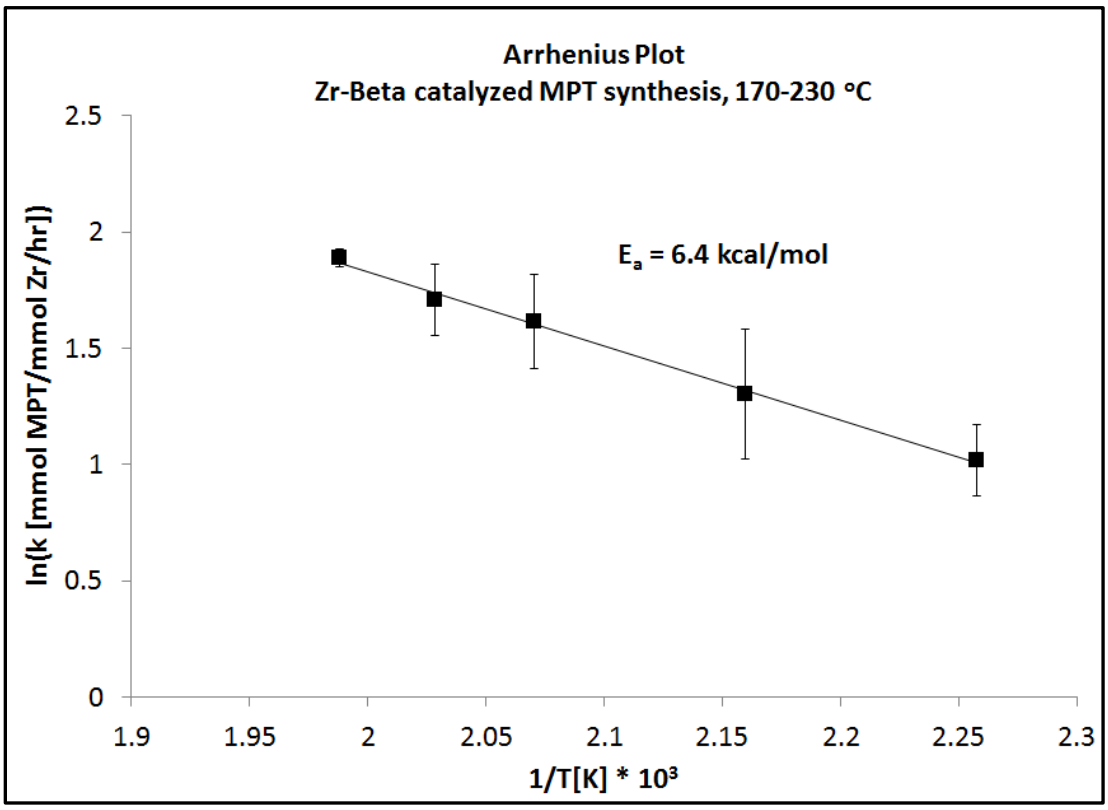

Fig. 7.11 Arrhenius Plot for Zr-Beta catalyzed MPT synthesis for 170-230^{o}C.

Table 7.6 Summary of measured apparent E_a's for PX and MPT synthesis using Zr-Beta catalyst.

Reaction	T (^{o}C)	E_a (kcal/mol)
DMF-PX	170-230	8.2 (avg)
	170-210	10.5
	210-230	1.9
MMF-MPT	170-230	6.4

7.3 Discussion of apparent E_a measurements for DMF/PX and MMF/MPT reactions using Zr-Beta.

All the apparent E_a measurements are summarized in Table 7.6. Since all four of these apparent E_a's are likely too low to be the true activation energy of a single chemical step, these data suggest the apparent E_a for the two processes may include a collection of terms that could result in low overall values. Since two chemical reactions are occurring in tandem (Diels-Alder cycloaddition and dehydrative aromatization) with the first reaction (Diels-Alder cycloaddition) possibly in thermodynamic equilibrium, it is reasonable to propose that the measured apparent E_a's are a combination of terms that may include, for example, the ΔH_{rxn} for the reversible Diels-Alder reaction, the true E_a for the dehydrative aromatization of the Diels-Alder adduct, and others. Additionally, ΔH_{ads} terms for adsorption steps in equilibrium (reactants or intermediates adsorbing reversibly onto the catalyst surface or active site) may be part of the apparent E_a's and could contribute to an overall low E_a value.

For example, a recent investigation by Patet, et al. on the Diels-Alder-dehydration of DMF and ethylene to produce PX using a Bronsted acid H-Y zeolite catalyst in heptane solvent showed a reaction regime in which the effective rate constant for the production of PX included multiple terms.[2] A simplified kinetic model for the H-Y catalyzed production of PX was proposed (Table 7.7) and the model was solved for a rate equation (Fig. 7.12). At low Bronsted acid active site concentrations this rate equation simplifies (Fig. 7.13),

showing that under these conditions the effect rate constant for PX production may include a collection of terms (k_2, K_1, K_4, K_6, etc.).

Table 7.7 Simplified kinetic model for the Diels-Alder-dehydration of DMF and ethylene to PX from Patet, et al. (2015).[2] Labels: DMF = dimethylfuran, E = ethylene, CA = Diels-Alder cycloadduct between DMF and E, PX = p-xylene, W = water, HDI = 2,5-hexanedione, * = Vacant strong acid H-Y site.

No.	Reactions
1	DMF + E $\rightleftharpoons$ CA
2	CA* $\longrightarrow$ PX + W*
3	DMF* + W $\rightleftharpoons$ HDI*
	Adsorption/Desorption steps
4	CA + * $\rightleftharpoons$ CA*
5	W + * $\rightleftharpoons$ W*
6	DMF + * $\rightleftharpoons$ DMF*
7	HDI + * $\rightleftharpoons$ HDI*

$$r_{PX} = \frac{k_2 K_1 K_4 [DMF][E][*]}{K_6(1 + K_3[W])[DMF] + \left(\frac{k_2}{k_{-1}}\right) K_4[*]}$$

Fig. 7.12 Rate of PX production using the simplified kinetic model in Table 7.7, reported in Patet, et al. (2015).[2] The parameters k_i and K_i are the reaction rate and equilibrium constants for reaction *i*, [i] is the concentration of component *i*, and [*] is the total Bronsted acid active site concentration.

$$r_{PX} = \left(\frac{k_2 K_1 K_4}{K_6(1 + K_3[W])}\right)[E][*]$$

Fig. 7.13 Reduced form of the PX production rate equation from Fig. 7.12 at low Bronsted acid active site concentrations, as reported in Patet, et al. (2015).[2]

Clearly, the conversions of DMF and MMF to PX and MPT with ethylene Diels-Alder-dehydration reactions are complex systems and additional investigation is required to provide deeper insight into the reaction mechanism.

7.4 Methods for determining initial rates

The measurement of PX yield was performed by GC/FID using triglyme as internal standard in dioxane solvent. Due to the similarity in boiling points, the DMF reactant elutes at the same time as dioxane in the GC. Therefore, DMF conversion (and PX selectivity) was unable to be determined by GC-FID. Quantitative ^{1}H NMR analysis was used to measure DMF conversion, and it was found that PX selectivities were ~40%. This is in agreement with previous reports of PX selectivity at low PX yields.[2] Due to the low PX selectivities at low yields, the PX yields were used (rather than DMF conversion) for determining the apparent E_a.

The MMF conversion and MPT yield was measured by GC/FID using triglyme as internal standard in dioxane solvent. The MMF conversion profiles at low conversion were unreliable and exhibited a larger amount of error. This was due to irreproducibility in the area ratio of the MMF/triglyme peaks in the gas chromatogram from injection to injection, and the source of the irreproducibility was unresolved. The area ratios of the MPT/triglyme peaks were very reliable from injection to injection and, therefore, the MPT yield profiles were used for determining the apparent E_a.

The plots in Fig. 7.14-15 show how initial rates were estimated using the collected PX and MPT yield profiles, including the maximum and minimum slopes used for reporting the error bars in Fig. 7.3, Fig. 7.5, Fig. 9, and Fig. 7.11.

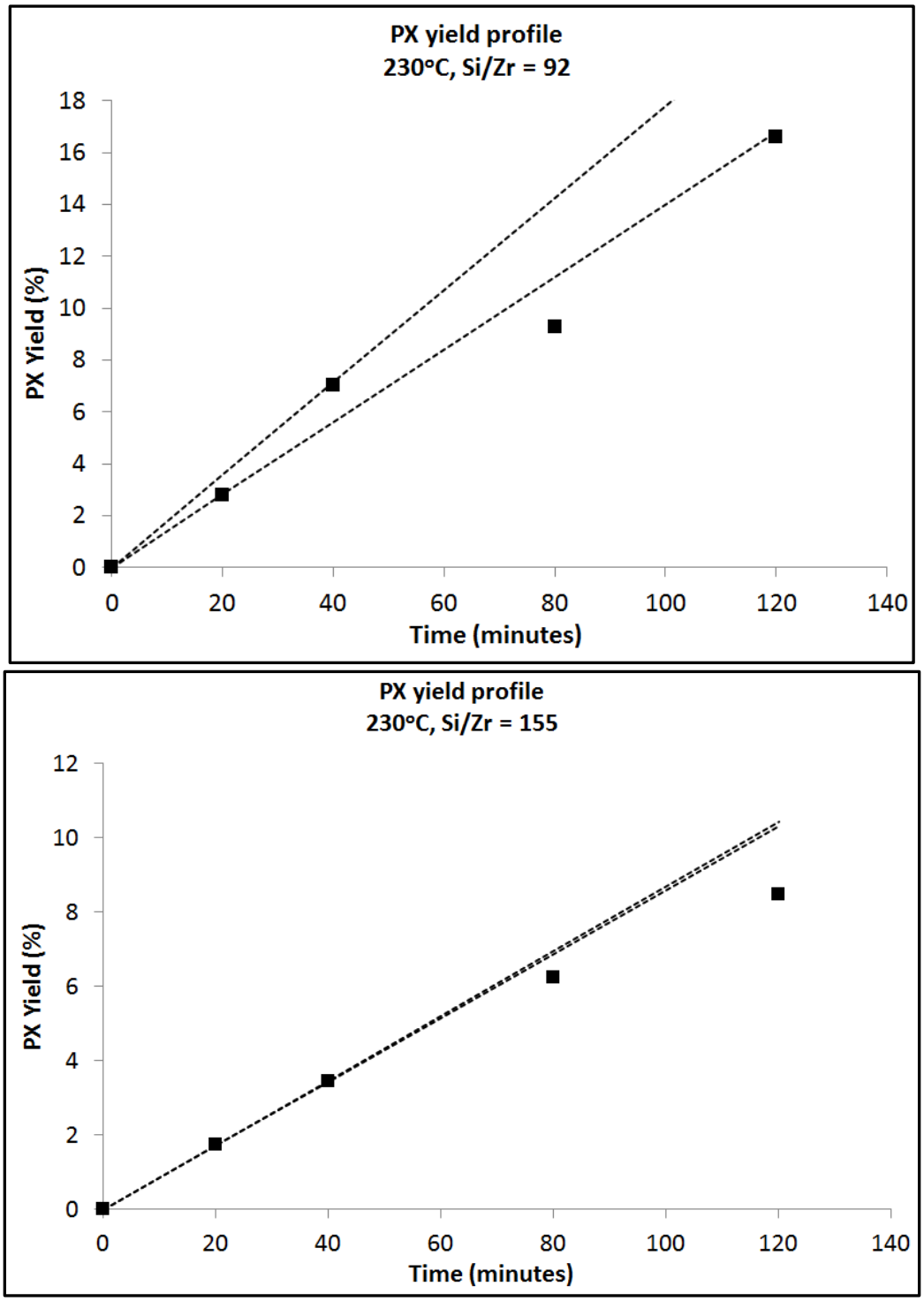

Fig. 7.14 Plots used for measuring the initial rates from the collected PX yield profiles.

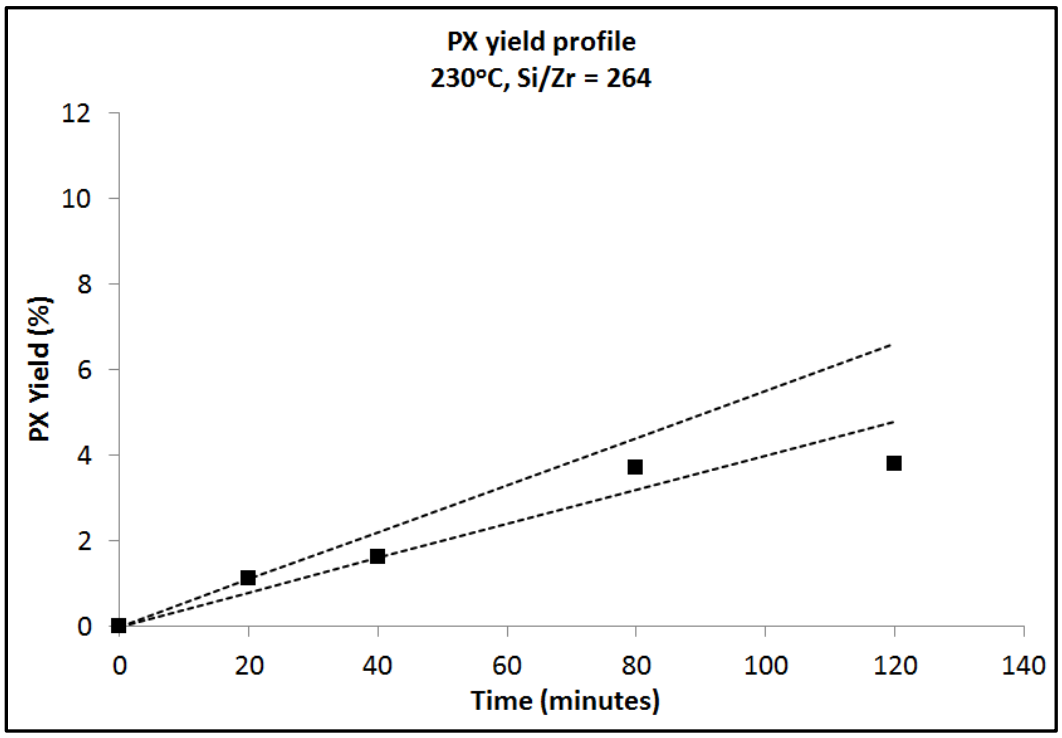

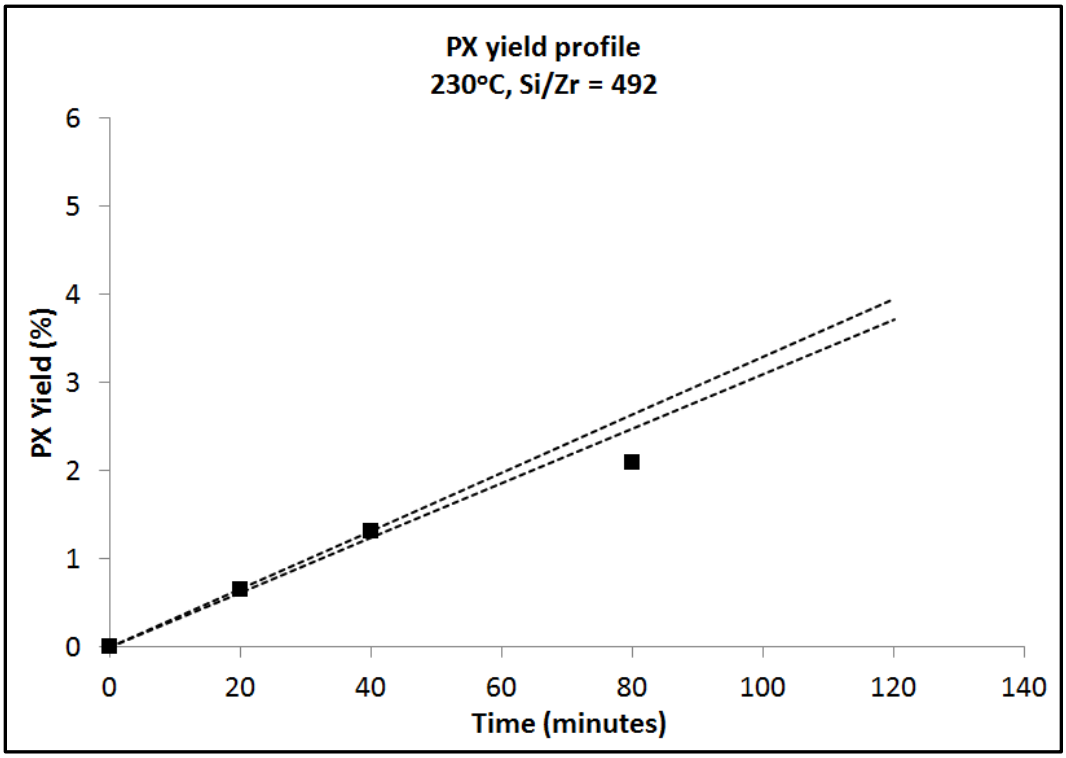

Fig. 7.14 continued. Plots used for measuring the initial rates from the collected PX yield profiles.

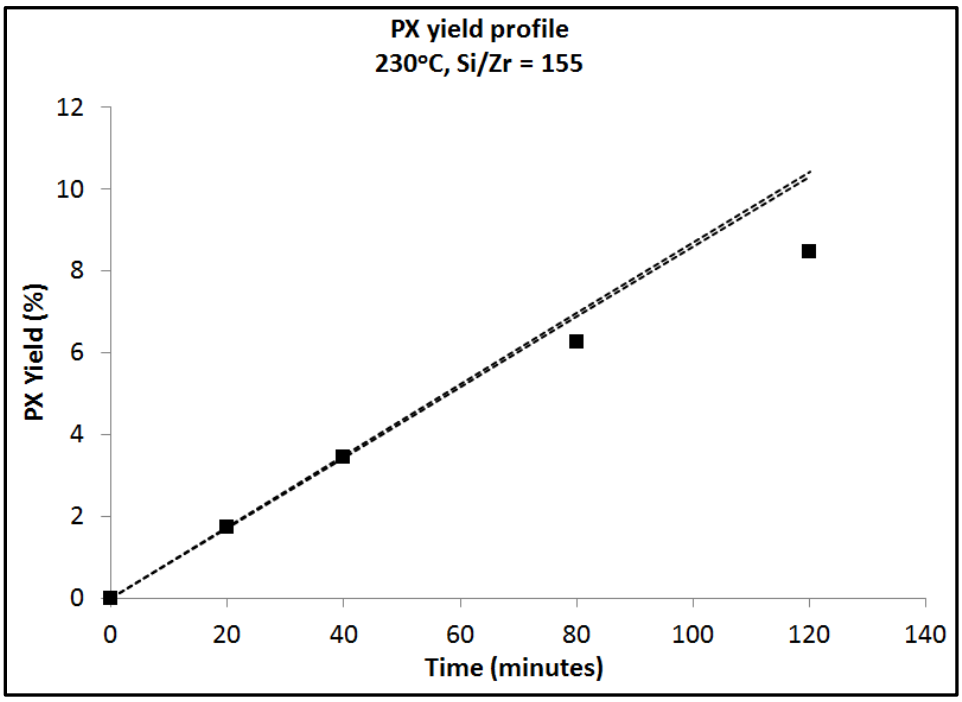

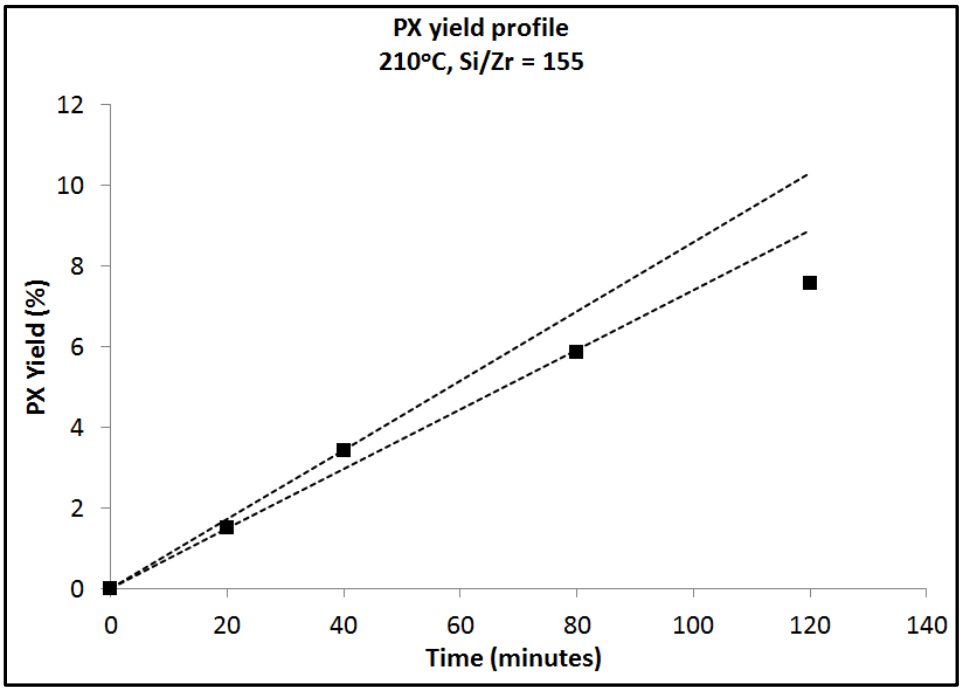

Fig. 7.14 continued. Plots used for measuring the initial rates from the collected PX yield profiles.

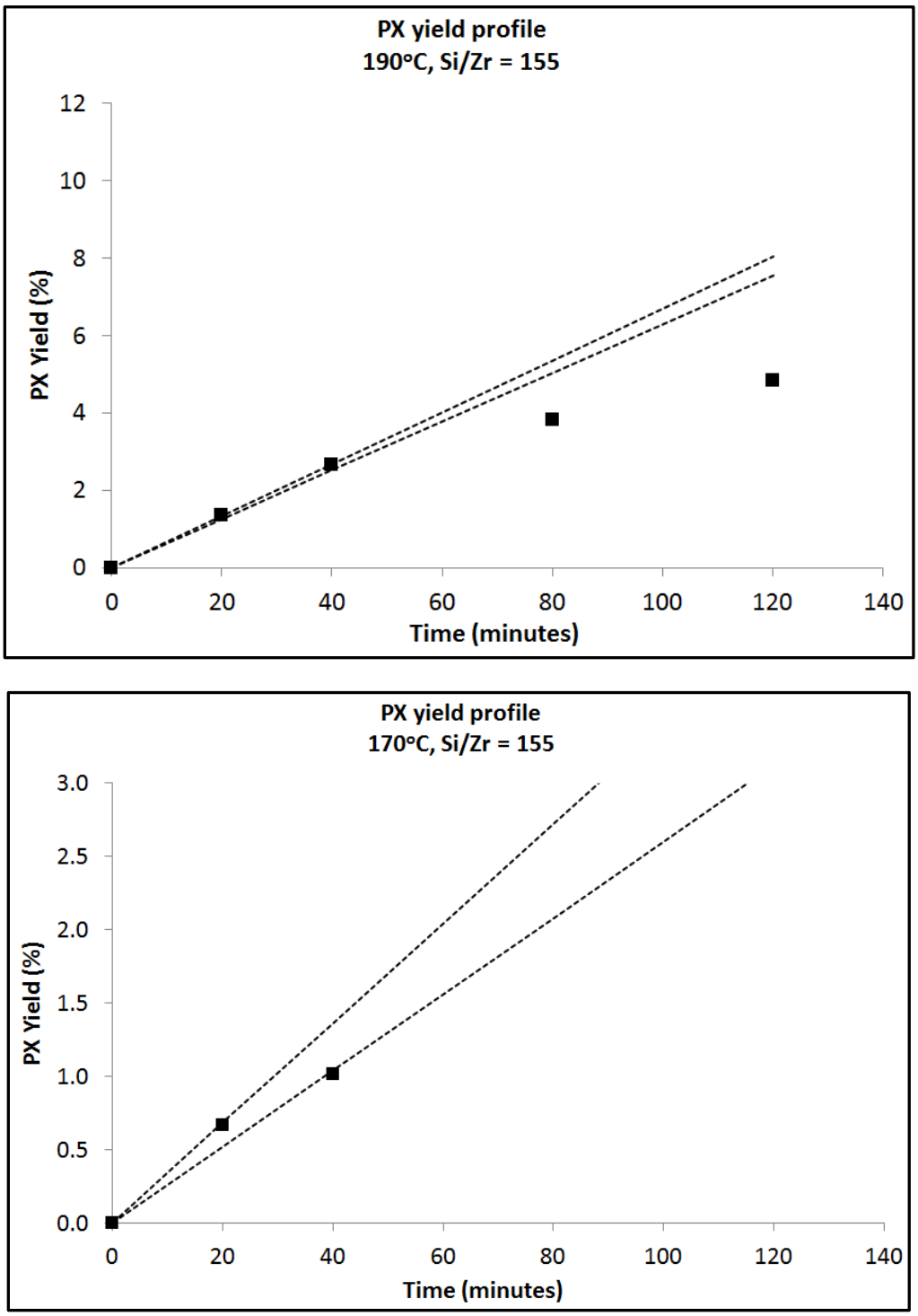

Fig. 7.14 continued. Plots used for measuring the initial rates from the collected PX yield profiles.

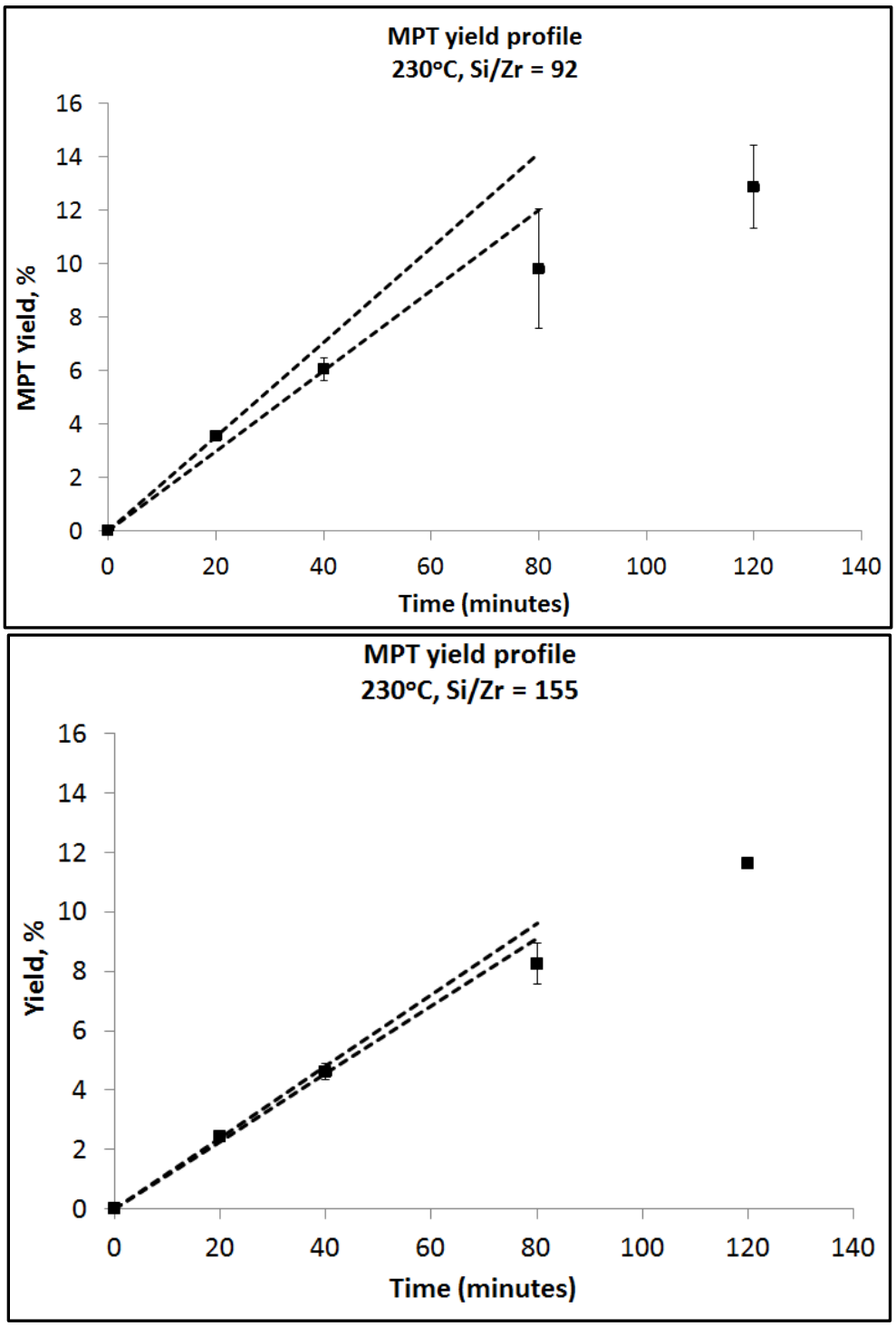

Fig. 7.15 Plots used for measuring the initial rates from the collected MPT yield profiles. Error bars are +/- standard deviation for multiple injections on GC.

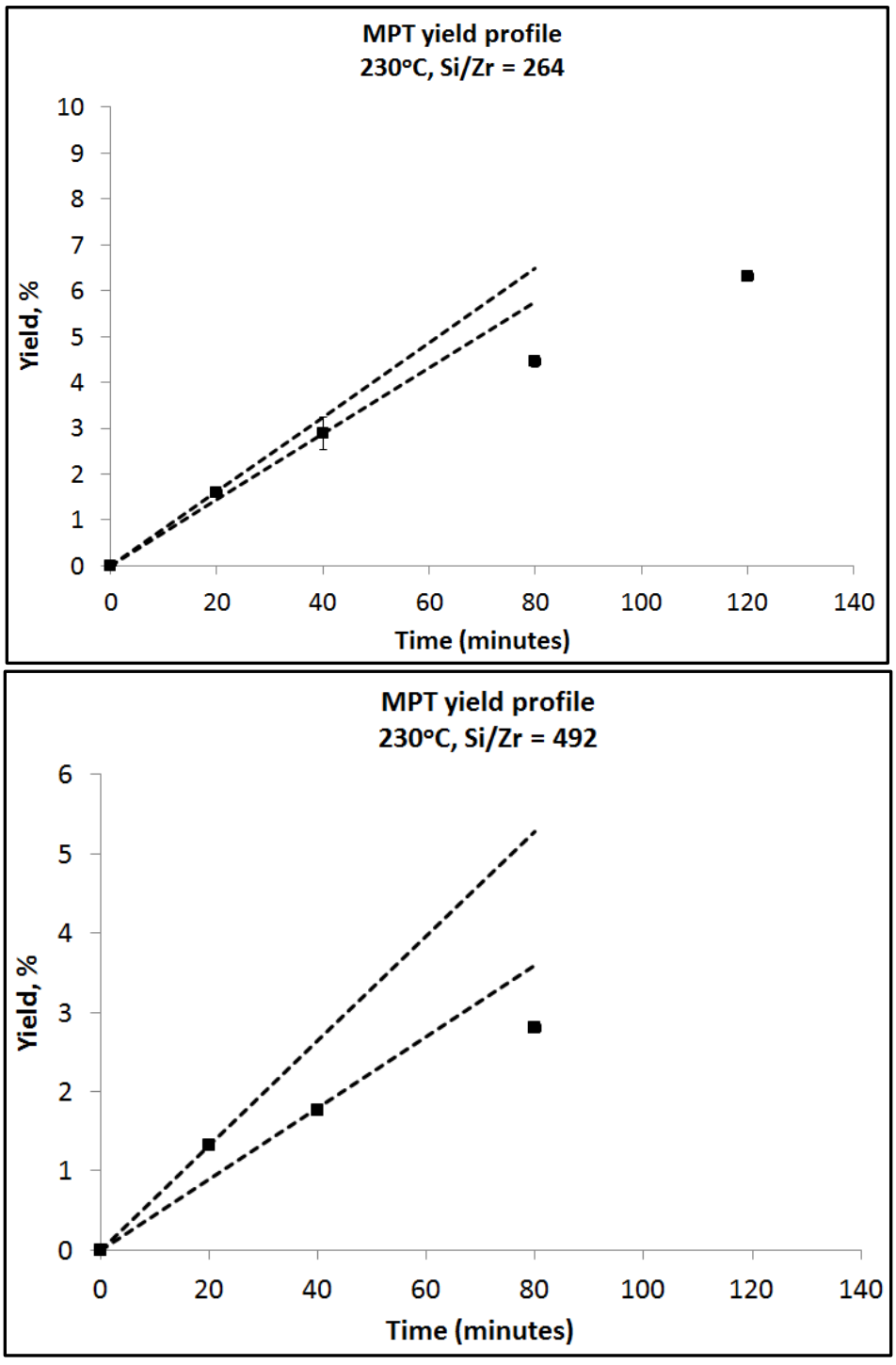

Fig. 7.15 continued Plots used for measuring the initial rates from the collected MPT yield profiles. Error bars are +/- standard deviation for multiple injections on GC.

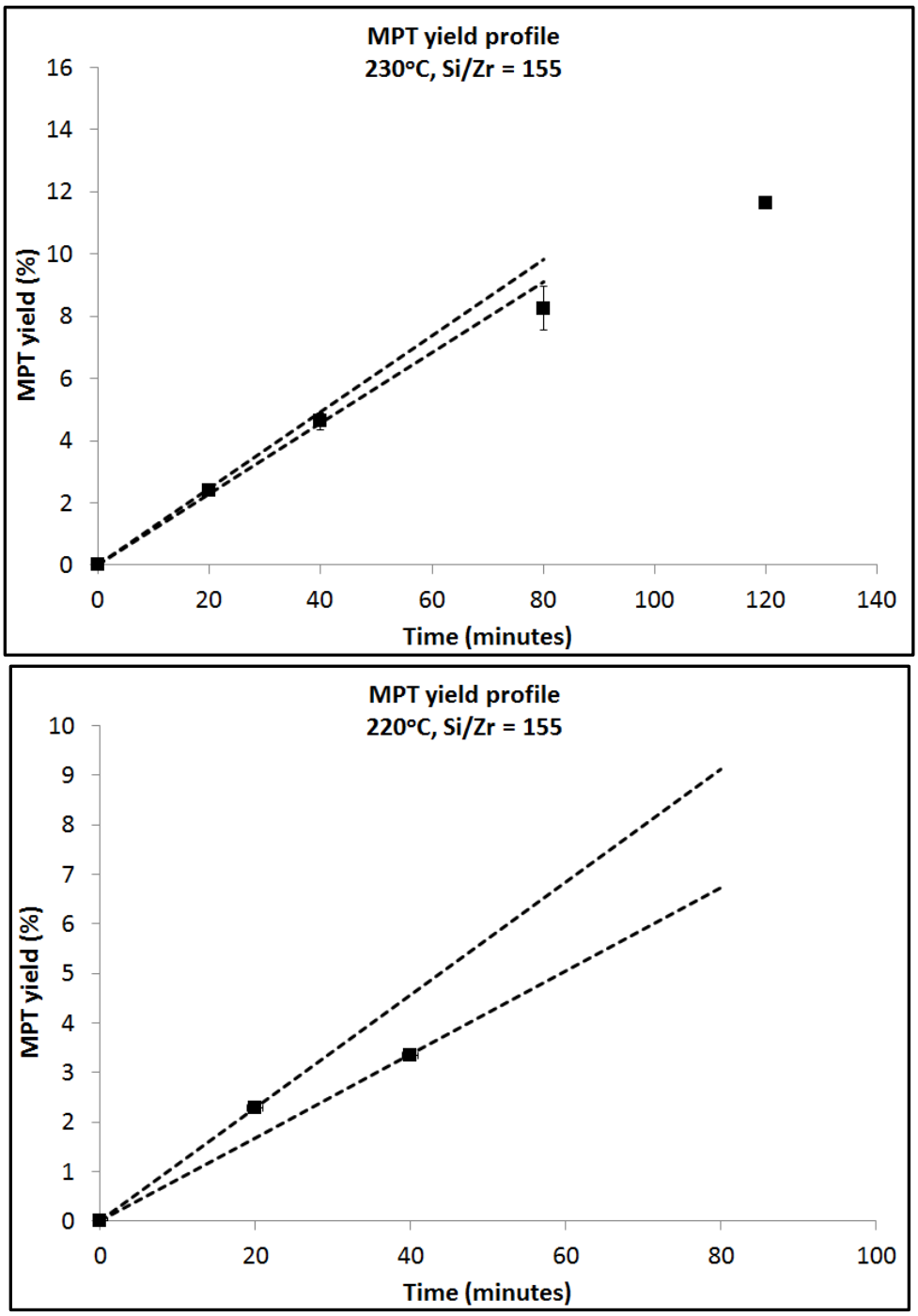

Fig. 7.15 continued Plots used for measuring the initial rates from the collected MPT yield profiles. Error bars at +/- standard deviation for yield determined by multiple injections on GC.

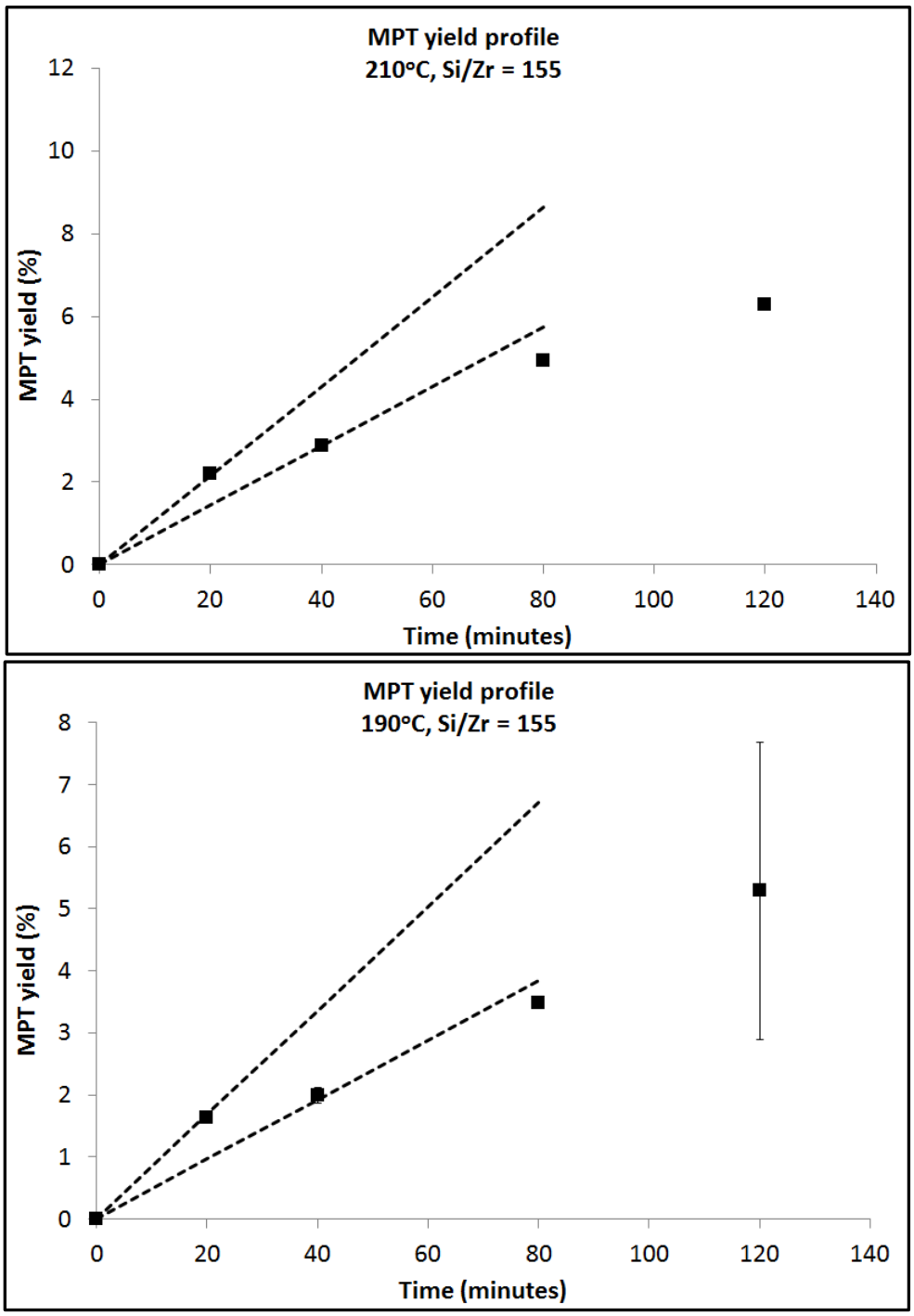

Fig. 7.15 continued Plots used for measuring the initial rates from the collected MPT yield profiles. Error bars at +/- standard deviation for yield determined by multiple injections on GC.

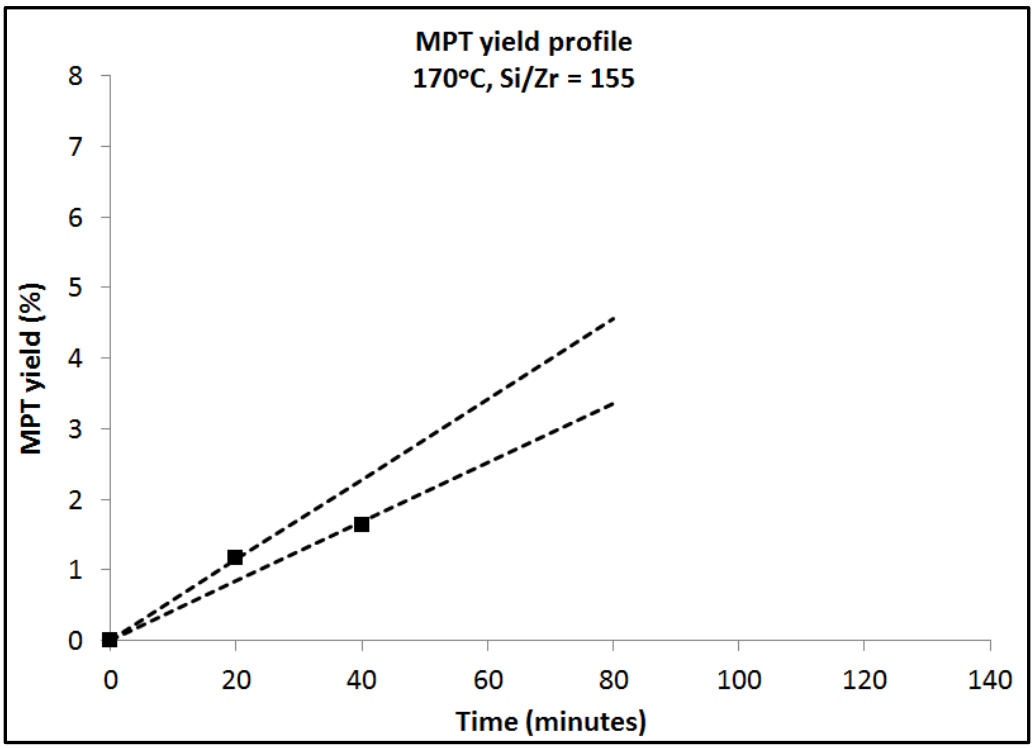

Fig. 7.15 continued Plots used for measuring the initial rates from the collected MPT yield profiles. Error bars at +/- standard deviation for yield determined by multiple injections on GC.

7.5 References

[1] Boudart, M.; *Chem. Rev.* **1995**, *95*, 661 – 666.

[2] Patet, R.E.; Nikbin, N.; Williams, C.L.; Green, S.K.; Chang, C-C.; Fan, W.; Caratzoulas, S.; Dauenhauer, P.J.; Vlachos, D.G.; *ACS. Catal.* **2015**, DOI: 10.1021/cs5020783.